

See discussions, stats, and author profiles for this publication at: <https://www.researchgate.net/publication/271608729>

High-resolution U–Pb dating of an Early Pleistocene stalagmite from Corchia Cave (central Italy)

Article in *Quaternary Geochronology* · December 2012

DOI: 10.1016/j.quageo.2012.10.005

CITATIONS

8

READS

64

5 authors, including:



Petra Bajo

University of Melbourne

13 PUBLICATIONS 38 CITATIONS

[SEE PROFILE](#)



Rn Drysdale

University of Melbourne

181 PUBLICATIONS 3,079 CITATIONS

[SEE PROFILE](#)



John C Hellstrom

University of Melbourne

191 PUBLICATIONS 4,364 CITATIONS

[SEE PROFILE](#)



Giovanni Zanchetta

Università di Pisa

297 PUBLICATIONS 5,453 CITATIONS

[SEE PROFILE](#)

Some of the authors of this publication are also working on these related projects:



Pleistocene palaeoclimate reconstructions from speleothem studies [View project](#)



Environmental changes in the Alps during the Holocene [View project](#)

All content following this page was uploaded by [Petra Bajo](#) on 14 July 2016.

The user has requested enhancement of the downloaded file. All in-text references [underlined in blue](#) are added to the original document and are linked to publications on ResearchGate, letting you access and read them immediately.



Research paper

High-resolution U–Pb dating of an Early Pleistocene stalagmite from Corchia Cave (central Italy)

Petra Bajo ^{a,*}, Russell Drysdale ^a, Jon Woodhead ^b, John Hellstrom ^b, Giovanni Zanchetta ^{c,d,e}^a Department of Resource Management and Geography, University of Melbourne, Parkville, 3010 Victoria, Australia^b School of Earth Sciences, University of Melbourne, Parkville, 3010 Victoria, Australia^c Department of Earth Sciences, University of Pisa, Pisa 56100, Italy^d Istituto di Georisorse e Geoscienza-CNR, Pisa 56100, Italy^e Istituto Nazionale di Geofisica e Vulcanologia, Pisa 56100, Italy

ARTICLE INFO

Article history:

Received 15 February 2012

Received in revised form

7 October 2012

Accepted 12 October 2012

Available online 24 October 2012

Keywords:

Uranium–lead (U–Pb) dating

Speleothems

Middle Pleistocene Transition

Corchia cave

Glacial terminations

ABSTRACT

Recent developments in the uranium–lead (U–Pb) dating of speleothems have opened up new opportunities in palaeoclimate research. An important goal in this new frontier is to produce palaeoclimate records underpinned by precise and accurate age models, which together will increase the range of palaeoclimate questions that can be addressed by the speleothem research community. In this paper, we investigate the level of age-model precision that is achievable by applying high-resolution U–Pb dating of a stalagmite (CC8) from Corchia Cave (Italy) whose period of growth spans part of the Middle Pleistocene Transition (~970–810 ka). Focussing largely on the periods encompassing three glacial terminations, we carried out age sampling of CC8 at a density similar to that performed in many studies of younger (i.e. U–Th-dated) speleothems. Using a combination of Tera–Wasserburg isochron and model age approaches, coupled with age–depth modelling, our results show that age-model uncertainties of ~4 kyr are possible, equivalent to a precision of about 0.4%. At this level of precision palaeoclimate time series derived from speleothems of this age can be used to test hypotheses of orbital forcing.

© 2012 Elsevier B.V. All rights reserved.

1. Introduction

Speleothems are well-established archives of palaeoenvironmental change (Fairchild et al., 2006; McDermott, 2004). The proxy data that underpin their utility in this regard are derived from the study of the physical and chemical properties of speleothem calcite, including the stable isotopes of oxygen and carbon (McDermott, 2004; Lachniet, 2009); trace elements (e.g. Mg, Sr and Ba – Borsato et al., 2007; Fairchild and Treble, 2009; Griffiths et al., 2010a; Hellstrom and McCulloch, 2000); growth rates and growth intervals (Baker et al., 1998; Baldini, 2010; Drysdale et al., 2005); strontium isotopes (Frumkin and Stein, 2004; Goede et al., 1998; Zhou et al., 2009); and fluid inclusions (Griffiths et al., 2010b; van Breukelen et al., 2008). The major strength of speleothems when compared to other palaeoclimate archives (e.g. deep-sea and ice cores), however, is that they can be accurately and precisely dated using the U-series decay scheme (Richards and Dorale, 2003), allowing palaeoclimate series to be fixed in absolute time.

Virtually all speleothem-based palaeoclimate studies up until now have been confined to the Middle to Late Pleistocene period because of the time constraints imposed by the practical upper limit of the U–Th dating method, i.e. ~500 ka (Richards and Dorale, 2003). Although advances in U-series isotopic measurements continue to push this boundary (Stirling et al., 2001; Cheng et al., 2009), the age of many speleothems clearly exceeds the U–Th limit (Walker et al., 2006; Woodhead et al., 2006, 2010). The possibility of probing the many important but unanswered questions in palaeoclimatology (and other fields, such as palaeoanthropology) using such older speleothems has traditionally been considered remote. However, recent refinement of the U–Pb dating method for speleothems has opened up new research opportunities in this field.

Since the publication of the first substantial paper on U–Pb dating of speleothems (Richards et al., 1998), the method has been improved, particularly in regards to screening procedures for sample selection, chemical separation, and sample-size requirements in response to the advent of multi-collector inductively coupled mass spectrometry (MC-ICP-MS) e.g. Woodhead et al. (2006, 2012). This has led to a rapid increase in the number of speleothem papers based around U–Pb dating. For example, U–Pb

* Corresponding author.

E-mail address: pbajo@student.unimelb.edu.au (P. Bajo).

dating of flowstones has been used to bracket the age of early hominin fossil-bearing sediments (de Ruiter et al., 2009; Pickering and Kramers, 2010; Pickering et al., 2010, 2011; Walker et al., 2006) and to determine rates of landscape evolution (Meyer et al., 2009, 2011; Polyak et al., 2008). Results of parallel dating of speleothems younger than 500 ka by U–Th and U–Pb methods have also been reported (Cliff et al., 2010), and a recent study has demonstrated that speleothems as old as the Permian can be successfully dated by U–Pb (Woodhead et al., 2010). Notwithstanding this recent upsurge of interest in speleothem U–Pb chronologies, so far no study has tested the limits of the method in terms of the age-model precision that might be accurately achieved. This is an important issue: in palaeoclimatology, in combination with isotope measurement accuracy, age-model precision and accuracy govern the specific palaeoclimate questions that speleothem studies are able to address.

Here we present the first high-resolution U–Pb chronology study of a single speleothem. Our principal aim is to explore the limiting precision achievable by applying a high density of age sampling comparable to that performed in studies of younger (U–Th dated) speleothems (Drysdale et al., 2009; Fleitmann et al., 2009). The stalagmite comes from Corchia Cave (central Italy) and grew during the Middle Pleistocene Transition, an interval during which the period of glacial–interglacial cycles apparently shifted from 40,000 yr to 100,000 yr (Raymo and Huybers, 2008). We demonstrate that levels of age-model uncertainty as low as 0.4–1.3%, equivalent to a few thousand years (95% confidence) are achievable after all sources of random and correlated uncertainty are considered, enabling the assembly of speleothem palaeoclimate records capable of testing competing hypotheses of climate forcing.

2. Study site and sample description

Corchia Cave is a ~60-km-long and ~1250-m-deep system located in the Alpi Apuane massif in central Italy (Fig. 1). The massif

is composed mainly of steeply dipping and complexly folded Mesozoic calcareous rocks (marbles and metadolostones). Large-scale structural features within the massif and a wet climate have permitted the development of one of the longest and deepest cave systems in Europe.

The object of this study is stalagmite CC8, which was recovered in three broken pieces from the upper part of the Galleria delle Stalattiti (GdS), situated 800 m from the nearest entrance and 400 m below the surface. The GdS is well decorated and is part of a 2 km-long tourist path. It experiences a very stable climate (Baneschi et al., 2011), and its speleothems have previously yielded important information on long- and short-term palaeoclimate events during the late Quaternary (Drysdale et al., 2004, 2005, 2007, 2009; Zanchetta et al., 2007). A key feature of these speleothems is the tendency for their stable isotope and trace element patterns to respond to changes in regional rainfall, which in turn are thought to be driven by changes in North Atlantic sea-surface temperatures (Drysdale et al., 2009).

The three pieces of CC8 have a combined length of 825 mm. The stalagmite is composed of translucent to opaque calcite, and is white to grey in colour (Fig. 2). Laminations are generally faint to absent to the naked eye, although one section towards the base displays a well-developed lamination pattern (Fig. 2c). There are no visible signs of diagenesis. However, along the stalagmite growth axis several potential growth hiatuses can be observed, as well as obvious changes in growth-axis direction. Although climate changes may be responsible for both, the effects of past earthquakes on the disruption of water flow paths in this seismically active region cannot be ruled out.

Exploratory U–Pb dating revealed that CC8 grew between ~810 ka and ~970 ka, and confirmed the presence of one significant hiatus that divides the speleothem into two main growth phases: 813 to 824 ka, and 873 to 968 ka. In this paper, we focus on the lower, older phase of stalagmite growth, which, based on a comparison with the deep-sea benthic oxygen isotope record, encapsulates three Middle Pleistocene glacial terminations.

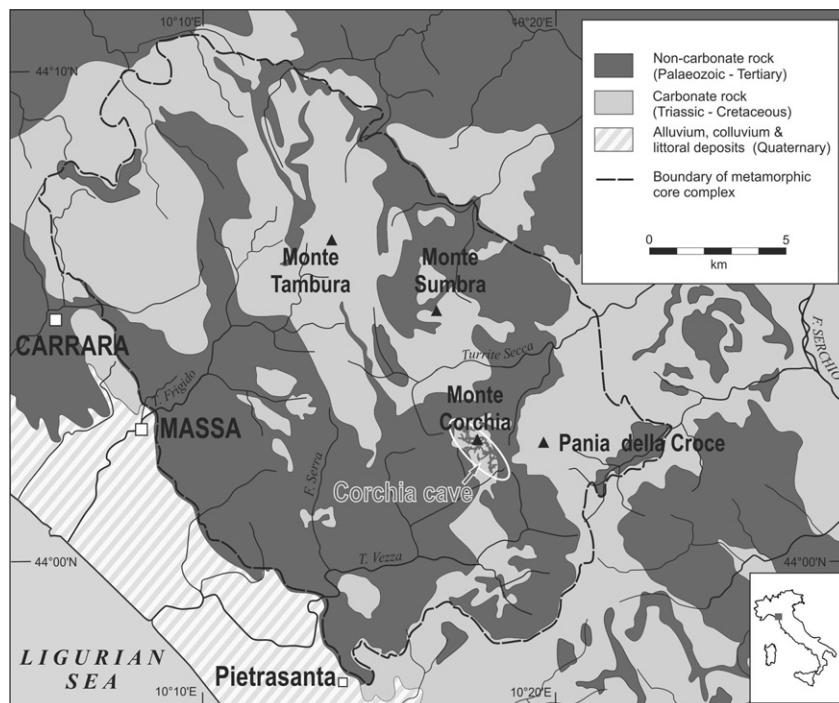


Fig. 1. Location of Corchia cave. (modified from Drysdale et al., 2004).

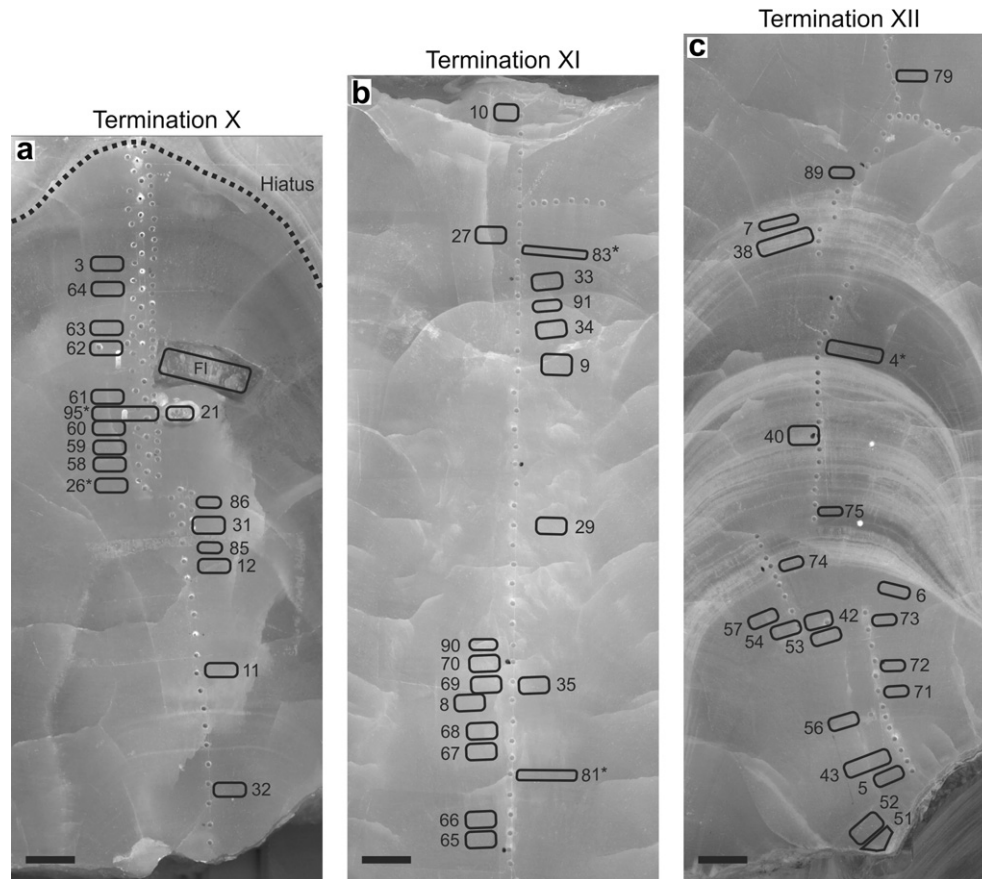


Fig. 2. Photograph of stalagmite CC8. Each plot (a, b, c) contains Terminations X, XI or XII as indicated on the figure. Numbered boxes are ($^{234}\text{U}/^{238}\text{U}$) measurements and U–Pb dating samples positions; the box labelled 'FI' is the position of a fluid-inclusion sample (not discussed in the text). Black scale bars are 1 cm in length.

A stable-isotope profile, which, together with other proxy measurements, is the subject of work in preparation, was used to determine the position of these glacial terminations and thus target the appropriate sections for intensive U–Pb dating.

3. Methods

3.1. Sampling

The three pieces of stalagmite CC8 were individually embedded in resin to prevent breakage during sample preparation then sectioned into slabs of 1–2 cm thickness for polishing. A total of 56 samples were extracted from the older 873 to 968 ka growth phase. For each sample $^{234}\text{U}/^{238}\text{U}$ analysis and U–Pb dating were performed. Of the total 56 samples, five were run as U–Pb isochron analyses, in which six to twelve prisms of calcite were extracted from a single growth segment as identified from the faint lamination patterns. Two isochron analyses were also carried out on the upper section of CC8.

For the U–Pb analyses, samples of between 50 and 200 mg were extracted either manually using a dental air drill or, after an upgrade of our speleothem sampling facility, by using a dental air drill fixed to a manually operated, video-guided X–Y–Z milling machine. In the former case, the samples were removed from the main slabs. For the video-guided sampling, smaller sections were cut from the main slabs and attached to the lathe's fixing plate. Two video cameras positioned along the X and Y stage axes of the lathe allowed for a high level of sampling precision to be achieved. Precise tracing of the laminations in the Z (vertical) axis was

achieved using a tilting sub-stage fitted to the fixing plate. Due to the high-intensity sampling and limited availability of speleothem, some samples were taken from the opposite side of the slabs. Lamination pattern-matching was used to place these samples on to a common depth scale. The sampling-depth uncertainties (which are used in the final age-depth model construction) for these samples were less than 0.5 mm.

For the $^{234}\text{U}/^{238}\text{U}$ measurements powdered samples were used. The powders were taken from the same depth position as corresponding U–Pb sample using a separate computer-guided micromilling machine (Drysdale et al., 2012).

3.2. U–Pb dating and $^{234}\text{U}/^{238}\text{U}$ analysis

U and Pb were chemically separated and analysed according to a slightly modified version of the method described in Woodhead et al. (2006). Briefly, aliquots were cleaned by two, short (1 min) immersions in very dilute ($\sim 0.1\text{M}$) HCl and washed in ultrapure water. The dried samples were dissolved in 6M HCl, and a mixed $^{233}\text{U}/^{205}\text{Pb}$ spike was added. After refluxing to ensure spike-sample equilibration and dry down, Pb and U were separated by conventional ion-exchange procedures. Full details of the method are contained in Woodhead et al. (2006) and Woodhead et al. (2012).

Isotope ratio analyses were performed on a Nu Plasma MC-ICP-MS equipped with a DSN desolvation unit and employing a Glass Expansion Opal Mist nebuliser uptaking at $\sim 50 \mu\text{L}/\text{minute}$. The NIST SRM 981 reference material for Pb and an internal $^{238}\text{U}/^{235}\text{U}$ ratio of 137.88 for U were used to monitor and correct for mass

Table 1
U–Pb and $^{234}\text{U}/^{238}\text{U}$ data from the lower portion of stalagmite CC8. Five samples with an asterisk are single-aliquot samples of the five isochron analyses from this portion of CC8. For the $^{234}\text{U}/^{238}\text{U}$ disequilibrium correction, ($^{234}\text{U}/^{238}\text{U}$) measurements are used. See text for further details.

Sample ID	Depth of prism centre from the top (mm)	$\pm 100\%$ error (mm)	Total Pb (ppb)	U (ppb)	$^{238}\text{U}/^{206}\text{Pb}$	$^{238}\text{U}/^{206}\text{Pb}$ 2 σ error (%)	$^{207}\text{Pb}/^{206}\text{Pb}$	$^{207}\text{Pb}/^{206}\text{Pb}$ 2 σ error (%)	($^{230}\text{U}/^{232}\text{U}$) (measured)	($^{234}\text{U}/^{238}\text{U}$) (measured)	($^{234}\text{U}/^{238}\text{U}$) (measured) 2 σ error	Age Ma (corr. for ($^{234}\text{U}/^{238}\text{U}$))	Age 2 σ error (Ma)
CC8-3	367	4	3.69	7935	4677	1.0	0.441	1.0	27,280	0.9771	0.0015	0.877	0.016
CC8-64	383.5	2.5	1.92	5372	5685	4.8	0.351	7.6	85,500	0.9799	0.0014	0.879	0.014
CC8-63	393	2.5	0.89	6321	8592	2.9	0.117	20	60,060	0.9790	0.0016	0.877	0.009
CC8-62	398	2.5	1.57	7202	7110	2.6	0.227	8.0	64,180	0.9822	0.0018	0.878	0.010
CC8-61	406	2.5	1.55	6709	7026	3.4	0.240	9.6	154,900	0.9816	0.0014	0.872	0.009
CC8-21	410	2	3.05	9329	5676	0.5	0.351	0.7	36,660	0.9816	0.0018	0.873	0.012
CC8-95*	410	2	1.44	7292	7787	7.0	0.174	30	58,080	0.9825	0.0011	0.871	0.012
CC8-60	413	2.5	2.06	7084	6139	1.4	0.313	2.6	31,900	0.9810	0.0013	0.875	0.010
CC8-59	417	2.5	2.70	6881	5187	1.5	0.389	2.0	91,920	0.9832	0.0012	0.869	0.011
CC8-58	419	2.5	1.17	6235	7578	2.1	0.191	7.9	69,450	0.9803	0.0021	0.882	0.012
CC8-26*	421	3	1.19	5881	7377	3.1	0.204	11	30,700	0.9821	0.0011	0.879	0.008
CC8-86	426	1	2.14	4899	5208	8.9	0.386	12	21,050	0.9820	0.0020	0.877	0.021
CC8-31	428	2.5	1.43	5956	6520	2.2	0.273	5.0	69,220	0.9830	0.0018	0.878	0.010
CC8-85	434	1.5	1.98	5877	5860	6.6	0.312	13	39,480	0.9853	0.0012	0.897	0.015
CC8-12	437.5	2	1.85	5934	5735	0.7	0.330	1.2	138,000	0.9841	0.0019	0.890	0.011
CC8-11	459.5	2	2.97	6912	4750	0.4	0.406	0.4	117,600	0.9850	0.0015	0.902	0.013
CC8-32	479	2	2.53	7631	5528	0.9	0.342	1.5	38,000	0.9849	0.0012	0.896	0.010
CC8-10	503	2	3.42	7343	4494	0.3	0.423	0.3	92,660	0.9869	0.0024	0.905	0.017
CC8-27	519.5	3.5	1.10	6124	7328	1.2	0.180	4.9	18,130	0.9850	0.0014	0.904	0.008
CC8-83*	531	2	1.49	6597	6991	5.0	0.207	17	51,060	0.9845	0.0017	0.911	0.012
CC8-33	537	2	2.33	5101	4576	0.7	0.425	0.8	40,330	0.9844	0.0019	0.895	0.016
CC8-91	542.5	2	2.80	7769	5460	3.4	0.346	5.5	81,380	0.9821	0.0010	0.914	0.012
CC8-34	546.5	2	3.37	7726	4732	0.4	0.415	0.5	105,500	0.9803	0.0018	0.911	0.015
CC8-9	556	2	2.07	6653	5711	0.3	0.325	0.3	48,240	0.9831	0.0020	0.907	0.013
CC8-29	586.5	2	5.88	8061	3343	0.4	0.527	0.3	133,500	0.9837	0.0010	0.914	0.021
CC8-70	613.5	2.5	1.82	6908	6355	2.0	0.270	4.8	78,690	0.9824	0.0014	0.910	0.011
CC8-90	616	1.5	1.36	7045	7664	7.4	0.150	37	39,760	0.9825	0.0011	0.920	0.013
CC8-69	617.5	2.5	1.83	6723	6230	1.7	0.280	3.8	29,150	0.9815	0.0017	0.917	0.012
CC8-35	619	2	1.55	5412	5934	1.4	0.304	2.8	54,100	0.9832	0.0013	0.910	0.010
CC8-8	622	2	0.80	5972	8131	0.6	0.112	3.8	54,560	0.9813	0.0022	0.923	0.014
CC8-68	627.5	2.5	1.38	5270	6440	3.8	0.256	9.6	55,850	0.9829	0.0014	0.919	0.012
CC8-67	631.5	2.5	2.19	4989	4779	2.2	0.398	2.8	26,390	0.9824	0.0017	0.929	0.016
CC8-81*	637	2	1.35	5034	6754	10	0.224	31	114,500	0.9842	0.0016	0.917	0.020
CC8-66	645	2.5	2.04	5229	5106	2.7	0.357	4.2	52,320	0.9854	0.0014	0.936	0.013
CC8-65	649	2.5	1.14	4600	6538	3.7	0.233	11	25,370	0.9836	0.0018	0.938	0.014
CC8-79	668	1.5	1.38	5129	6354	6.2	0.232	18	79,380	0.9874	0.0014	0.945	0.014
CC8-89	689	1.5	1.51	5743	6463	7.2	0.218	23	79,510	0.9858	0.0021	0.962	0.018
CC8-7	696	2	4.46	5547	3093	2.0	0.535	1.4	12,000	0.9878	0.0013	0.937	0.023
CC8-38	701	2.5	2.49	5651	4677	2.7	0.382	3.8	25,360	0.9889	0.0021	0.947	0.017
CC8-4*	720.5	3.5	2.28	4470	4286	3.1	0.420	3.6	21,690	0.9879	0.0021	0.950	0.018
CC8-40	741	2.5	4.63	4595	3651	1.6	0.485	1.0	53,270	0.9844	0.0017	0.957	0.021
CC8-75	756	1.5	2.93	4922	3954	4.8	0.453	4.8	63,140	0.9870	0.0019	0.951	0.021
CC8-74	767	2	4.98	4815	2567	1.7	0.580	1.0	43,820	0.9863	0.0022	0.961	0.033

CC8-6	773	2	1.38	4454	5472	0.9	0.298	1.8	58,760	0.9887	0.0011	0.966	0.010
CC8-57	775.5	2.5	1.55	5677	5984	2.3	0.253	5.8	32,970	0.9896	0.0019	0.953	0.013
CC8-54	780	2.5	1.61	5652	5400	1.7	0.307	3.3	39,110	0.9884	0.0022	0.964	0.016
CC8-42	781	2	2.19	5708	4881	1.0	0.356	1.5	16,450	0.9885	0.0017	0.965	0.013
CC8-73	782.5	2	2.77	6072	4648	5.2	0.375	7.4	79,030	0.9875	0.0016	0.977	0.019
CC8-53	784	2.5	1.34	5473	6278	1.9	0.227	5.7	39,960	0.9891	0.0021	0.954	0.014
CC8-72	793	1.5	2.27	6022	5236	6.5	0.313	12	21,630	0.9906	0.0017	0.969	0.018
CC8-71	799	1.5	2.67	5046	4166	3.3	0.421	3.9	93,900	0.9879	0.0019	0.977	0.019
CC8-56	802.5	2.5	2.17	4705	4488	2.5	0.387	3.4	10,010	0.9892	0.0010	0.975	0.013
CC8-43	807.5	2.5	4.05	6109	6137	1.8	0.230	4.5	23,030	0.9912	0.0014	0.959	0.009
CC8-5	813.5	2	1.76	5427	5534	4.0	0.285	8.8	30,160	0.9908	0.0012	0.965	0.011
CC8-52	818	2.5	1.46	6094	6353	3.4	0.206	12	14,170	0.9900	0.0016	0.970	0.012
CC8-51	821.5	2.5	1.27	5983	6617	2.4	0.184	9.3	35,080	0.9899	0.0012	0.966	0.009

fractionation effects. Total Pb blanks were typically in the range 5–10 pg and appropriate blank corrections, coupled with isotope-dilution calculations, were made using the Schmitz and Schoene (2007) algorithm.

Isochrons were constructed from five sample positions in the older section and two sample positions in the younger section of CC8, and were used to assess the composition and variability of the common Pb component present. Thereafter, ages were determined from single-sample aliquots using the common-Pb corrected model age methods outlined in Woodhead et al. (2012).

For $^{234}\text{U}/^{238}\text{U}$ analysis, samples of ca. 5 mg were prepared and analysed following the U–Th method described by Hellstrom (2003). Powder samples dissolved in concentrated HNO_3 to which a mixed ^{236}U – ^{233}U – ^{229}Th isotopic spike was added. After overnight refluxing, ion-exchange chemistry was employed for U and Th separation.

The samples were analysed on a Nu Plasma MC-ICP-MS, with frequent repeat measurements of the uranium isotopic standard NBL-112A used to determine external $^{234}\text{U}/^{238}\text{U}$ variability, then propagated into the reported uncertainties.

3.3. Age-depth model calculation

U–Pb data were interpolated versus depth using a Monte-Carlo simulation of a finite positive growth-rate model (Drysdale et al., 2004, 2005; Hendy et al., 2012; Scholz et al., 2012). For each iteration of the Monte-Carlo simulation all dates were randomised with respect to their uncertainties, and a least-squares fit obtained of a series of line segments such that growth rate is always finite and positive with an additional weighting to minimise its variation between segments. After 10,000 iterations all model outputs were ranked at each of 500 depths to construct curves for the 97th, 50th and 3rd percentiles of the model. All age model outputs are reported and discussed in terms of (typically asymmetric) 95% confidence intervals.

3.4. Age model accuracy and precision

Until recently (Scholz et al., 2012) there has been little discussion of how speleothem age models should be produced, and the question of accuracy versus precision remains largely unaddressed. Existing age models treat all uncertainty as random as is expected from measurement uncertainty, however there may also be correlated, systematic sources of uncertainty present such as in decay constants, tracer calibration, isotopic compositions etc. Although these sources of uncertainty are usually included in the calculation of individual ages, overlapping densely sampled ages can lead to overly precise age model uncertainties. Because of this, it might sometimes be necessary to quarantine the effects of known, correlated uncertainties during age model generation and add them to the resulting uncertainty envelope afterwards.

4. Results

4.1. U and Pb concentrations

The U–Pb dating results are presented in Tables 1 and 2. As with earlier studies on younger Corchia speleothems (e.g. Drysdale et al., 2005, 2009; Zanchetta et al., 2007), the radiometric analyses revealed high U concentrations: ~3.8–11.3 ppm. The Pb concentrations are very low, ranging from ~0.8–6.1 ppb. Again, this mirrors our previous observations regarding the relatively clean nature of Corchia speleothems, as determined from low Th concentrations recorded in U–Th-dated samples. Additional evidence for the purity of stalagmite CC8 is recorded in extremely

Table 2
U and Pb data for seven isochrons measured along the whole section of stalagmite CC8. The common Pb composition has been used to calculate single-point isochron ages following the method of Woodhead et al. (2012). The samples with an asterisk correspond to the samples for each isochron which have been used as the input ages in the age-depth modelling.

Sample ID	Depth of prism centre from the top (mm)	± 100% error (mm)	Total Pb (ppb)	U (ppb)	²³⁸ U/ ²⁰⁶ Pb	²³⁸ U/ ²⁰⁶ Pb 2σ error (%)	²⁰⁷ Pb/ ²⁰⁶ Pb	²⁰⁷ Pb/ ²⁰⁶ Pb 2σ error (%)	MSWD ^a	(²³⁴ U/ ²³⁸ U) (measured)	(²³⁴ U/ ²³⁸ U) (measured) 2σ error	Age Ma (corr. for (²³⁴ U/ ²³⁸ U) _i)	Age error 2σ (Ma)
CC8-1	5.0	2.0							54				
CC8-1-1			2.54	9974	6767	0.4	0.309	0.7					
CC8-1-2			1.69	7706	7296	0.7	0.272	1.6					
CC8-1-3			2.30	8396	6514	0.5	0.327	0.8					
CC8-1-4			1.10	6524	8161	1.0	0.200	3.4		0.9762	0.0020	0.822	0.011
CC8-1-5			2.40	8022	6192	0.5	0.349	0.8					
Isochron age												0.820	0.060
CC8-2	187.5	2.5							7.5				
CC8-2-1			1.0	9237	9134	1.1	0.105	8.1		0.9800	0.0020	0.833	0.009
CC8-2-2			1.32	9349	8407	0.9	0.161	4.2					
CC8-2-3			1.95	11,268	7802	0.8	0.211	2.5					
CC8-2-4			2.06	11,252	7609	0.8	0.224	2.6					
CC8-2-5			2.02	10,325	7411	0.7	0.240	1.9					
Isochron age												0.833	0.024
CC8-95	410.0	2.0							13				
CC8-95-1			2.38	8206	6285	3.5	0.300	7.2					
CC8-95-2			2.14	7873	6619	5.8	0.269	14					
CC9-95-3			2.13	8005	6685	6.2	0.255	16					
CC8-95-4			2.91	8225	5555	1.9	0.358	3.0					
CC8-95-5			1.83	7698	7029	4.9	0.237	14					
CC8-95-6			3.26	8198	5212	1.9	0.394	2.4					
CC8-95-7*			1.44	7292	7787	7.0	0.174	30		0.9825	0.0011	0.871	0.011
CC8-95-8			2.35	7488	6037	3.6	0.325	6.4					
CC8-95-9			2.40	8150	6095	1.9	0.310	3.7					
CC8-95-10			3.43	7964	4868	1.1	0.413	1.3					
CC8-95-11			3.14	8109	5217	1.6	0.383	2.2					
CC8-95-12			2.56	7949	5928	3.4	0.331	6.0					
Isochron age												0.876	0.014
CC8-26	421.0	3.0							65				
CC8-26-1			1.76	5626	5792	0.5	0.336	0.8					
CC8-26-2			1.14	5793	7262	0.6	0.217	1.9					
CC8-26-3			1.10	5531	7216	0.5	0.218	1.6					
CC8-26-4			1.24	5441	6816	0.4	0.255	1.1					
CC8-26-5*			1.19	5881	7377	3.1	0.204	11		0.9821	0.0011	0.879	0.008
CC8-26-6			1.30	5951	7204	3.9	0.217	13					
Isochron age												0.877	0.016
CC8-83	531.0	2.0							5.5				
CC8-83-1			2.37	6691	5504	4.3	0.331	7.5					
CC8-83-2			2.58	6641	5193	3.8	0.357	5.9					
CC8-83-3			2.49	6786	5449	5.0	0.338	8.5					
CC8-83-5			2.13	6926	5898	3.2	0.300	6.4					
CC8-83-6			2.27	6896	5707	2.7	0.327	4.8					
CC8-83-7			1.41	6261	7537	13	0.158	60					
CC8-83-8*			1.49	6597	6991	5.0	0.207	17		0.9845	0.0017	0.911	0.012
CC8-83-9			2.05	6943	5979	2.6	0.293	5.4					
CC8-83-10			2.33	6851	5626	4.2	0.321	7.6					

Isochron age	637.0	2.0	4.35	5446	3218	2.9	0.541	2.0	6.9	0.917	0.0016	0.9842	0.020	0.908	0.019
CC8-81															
CC8-81-1			4.99	5476	2904	3.0	0.562	1.9							
CC8-81-2			2.51	5268	4677	5.2	0.408	6.4							
CC8-81-3			4.04	5432	3373	3.1	0.519	2.3							
CC8-81-4			2.53	5164	4620	4.9	0.425	5.6							
CC8-81-5			1.35	5034	6754	10.0	0.224	30							
CC8-81-6*			5.23	5060	2622	3.1	0.580	1.8							
CC8-81-7			6.11	5042	2299	2.8	0.608	1.4							
CC8-81-8			5.82	5107	2424	3.0	0.597	1.6							
CC8-81-9															
Isochron age	720.5	3.5	2.23	4216	4053	0.4	0.437	0.4	18	0.915	0.0021	0.9879	0.018	0.947	0.045
CC8-4			2.47	4187	3764	0.4	0.462	0.3							
CC8-4-1			2.37	4087	3806	0.3	0.459	0.3							
CC8-4-2			2.20	4076	3993	0.4	0.442	0.4							
CC8-4-3			2.07	3961	4085	0.4	0.435	0.4							
CC8-4-4			2.44	3779	3541	0.5	0.484	0.4							
CC8-4-5			2.62	3823	3472	1.6	0.494	1.3							
CC8-4-6			2.45	4416	4012	2.2	0.441	2.3							
CC8-4-7			2.28	4470	4286	3.1	0.420	3.6							
CC8-4-8															
CC8-4-9*															

* Note: the MSWDs are calculated by Isoplot (Ludwig, 2001) based upon the assumptions of a model 2 fit, i.e. by assigning equal weights and zero error correlations to each point.

high $^{230}\text{Th}/^{232}\text{Th}$ activity ratios measured for all of 56 samples with the minimum value greater than 10,000 (Table 1). As noted by Woodhead et al. (2006), who reported the U–Pb age of another Corchia speleothem (CC16), the combination of high U and low Pb presents significant advantages for U–Pb chronologies and confines the major source of final age uncertainty to the initial uranium disequilibrium correction. We minimised this limitation by measuring $^{234}\text{U}/^{238}\text{U}$ activity ratios for each U–Pb sample position.

4.2. Raw U–Pb data and disequilibrium-corrected ages

4.2.1. Isochron age results

The seven isochron age results are shown in Table 2 and Fig. 3. As reported in Woodhead et al. (2012), single-aliquot U–Pb ages are a possible alternative to the more labour-intensive isochron ages in cases where the speleothem is highly radiogenic (i.e. with high $^{238}\text{U}/^{206}\text{Pb}$, where measured samples occupy a position relatively close to concordia) and where the isotopic composition ($^{207}\text{Pb}/^{206}\text{Pb}$ ratio) of the common-Pb end member is well constrained. If these two criteria are met, the individual aliquot ages should be statistically indistinguishable from the isochron age. $^{207}\text{Pb}/^{206}\text{Pb}$ intercept values for all seven isochrons are within error of each other (Fig. 4), which is indicative of a consistent net source of common Pb throughout the growth of the stalagmite. The robust median of all seven isochron y-intercepts and their uncertainties gives an estimate of the common Pb composition of $0.818 \pm 0.006/-0.011$ (98.4% confidence).

4.2.2. $^{234}\text{U}/^{238}\text{U}$ results and secular disequilibrium correction

Due largely to weathering and hydrological processes, speleothems are always deposited out of secular isotopic equilibrium with respect to the initial $^{234}\text{U}/^{238}\text{U}$ activity, i.e. $(^{234}\text{U}/^{238}\text{U})_i \neq 1$ (Richards and Dorale, 2003). The age effect of this disequilibrium (when compared to the more traditional U–Pb assumption of U-series equilibrium at the time of deposition) can amount to more than 100 ka and thus its accurate quantification is very important for samples of a few Ma or less in age (Ludwig, 1977; Richards et al., 1998; Woodhead et al., 2006). For a given U–Pb sample, such a correction is based on an estimate of the $(^{234}\text{U}/^{238}\text{U})_i$, which for relatively young samples can be quantitatively derived from direct measurement of $(^{234}\text{U}/^{238}\text{U})$ within the calcite. For the latter, we performed $(^{234}\text{U}/^{238}\text{U})$ measurements on all U–Pb samples from the older portion of CC8 (Table 1, Fig. 5). $(^{234}\text{U}/^{238}\text{U})$ values varied from 0.9771 ± 0.0015 to 0.9912 ± 0.0013 during the ~100 kyr-long growth period of this section of CC8. These values are low compared to those of speleothems from most other cave systems (Richards and Dorale, 2003), but consistent with previous U–Th studies at Corchia (Drysdale et al., 2009). Although the overall trend of $(^{234}\text{U}/^{238}\text{U})$ is decreasing with time, our high density of sampling reveals that this is not monotonic: we observe significant variability in $(^{234}\text{U}/^{238}\text{U})$ that likely reflects changing hydrological conditions during different climate states. This is currently the subject of ongoing study.

4.2.3. U–Pb age calculation

Disequilibrium-corrected, single-aliquot U–Pb ages were determined by projecting an assumed initial $^{207}\text{Pb}/^{206}\text{Pb}$ through the measured $^{207}\text{Pb}/^{206}\text{Pb}$ – $^{238}\text{U}/^{206}\text{Pb}$ point onto a disequilibrium concordia corresponding to measured $^{234}\text{U}/^{238}\text{U}$, and assuming complete initial exclusion of all other daughter products (Woodhead et al., 2006). All inputs are randomised with respect to their uncertainties, taking account of measured $^{207}\text{Pb}/^{206}\text{Pb}$ – $^{238}\text{U}/^{206}\text{Pb}$ error correlation, during a 1000-point Monte-Carlo simulation from which age and its 95% uncertainty are determined.

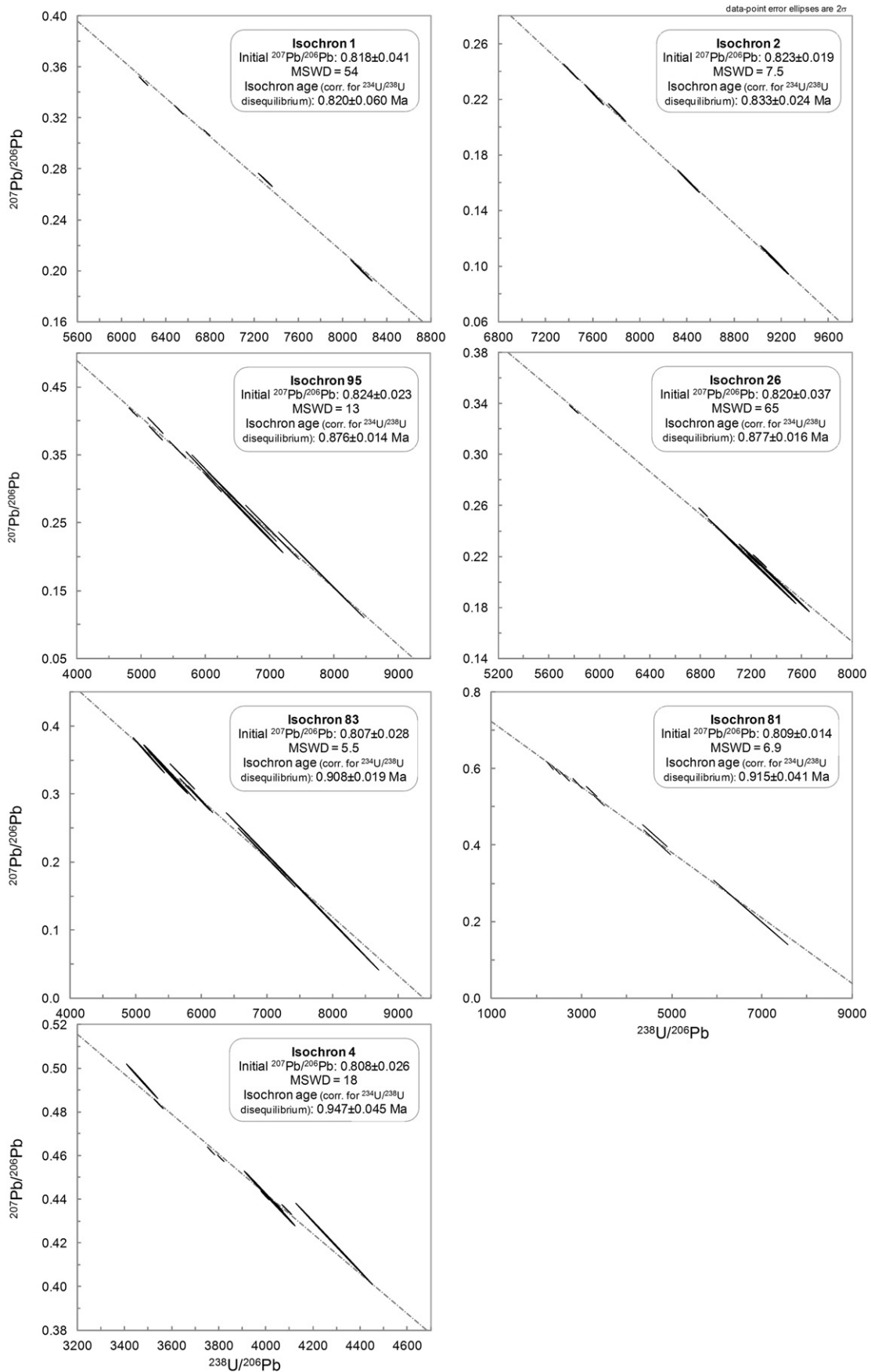


Fig. 3. Plots for seven full isochrons determined for CC8 and constructed using Isoplot (Ludwig, 2001). NB: the x- and y-axis ranges are different for each plot.

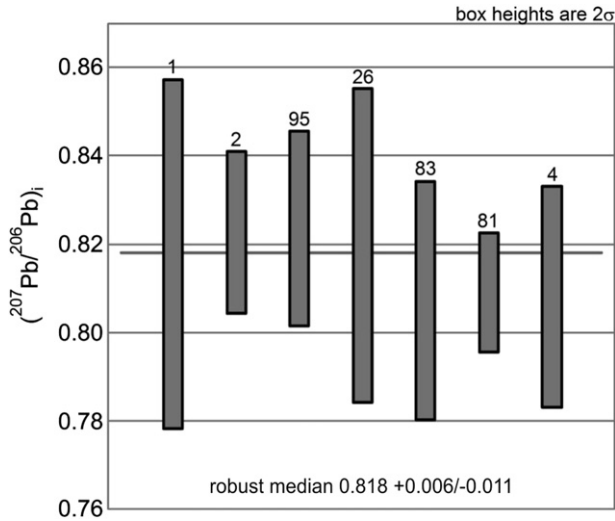


Fig. 4. $^{207}\text{Pb}/^{206}\text{Pb}$ intercept values for all seven isochrons are within error of each other, suggesting a consistent source of common Pb. The robust median for this common Pb composition is $0.818 + 0.006/-0.011$ (98.4% confidence), indicated by the thick horizontal line.

The final U–Pb ages for the lower part of CC8 are plotted versus depth in Fig. 6. Although this plot shows some degree of age scatter with depth, all U–Pb analyses returned ages in stratigraphic order when viewed within the constraints of the combined age uncertainties of stratigraphically successive sample pairs. A finite positive-growth-rate age-depth model determined through these data gave an MSWD of 0.62 indicating that, if anything, their uncertainties had been overstated. Removing the assigned uncertainty of the common Pb $^{207}\text{Pb}/^{206}\text{Pb}$ from the ages gives an age-model MSWD of 1.05. Varying the assigned $^{207}\text{Pb}/^{206}\text{Pb}$ yields a minimum MSWD of 1.03 at 0.8195, giving a stratigraphically-constrained (Hellstrom, 2006), best-fit initial $^{207}\text{Pb}/^{206}\text{Pb}$ well within the range determined by isochron analyses. A conservative uncertainty of ± 0.010 was assigned on the basis of both approaches.

4.3. Age uncertainties and age-depth modelling

A finite, positive-growth-rate age-depth model was determined through the entire population of single-aliquot U–Pb ages. A feature of this and other commonly used speleothem age-depth models (Scholz et al., 2012) is that all age uncertainty is treated as independent, and as such increasing age measurement density leads to increasingly higher-precision models, with no limit. Here, the isochron-dependent initial common $^{207}\text{Pb}/^{206}\text{Pb}$ value assigned to the single-aliquot ages is taken to be invariant between samples, and any error in our determination of it will affect all of them in a systematic manner. To address this, a component of the assigned $^{207}\text{Pb}/^{206}\text{Pb}$ uncertainty (of ± 0.007) was removed from the U–Pb ages prior to age-model calculation using $^{207}\text{Pb}/^{206}\text{Pb} = 0.8195 \pm 0.0070$. Two additional age models were determined for ages calculated with $^{207}\text{Pb}/^{206}\text{Pb}$ of 0.8125 ± 0.0070 and 0.8265 ± 0.0070 , and their differences from the original model were calculated along their lengths. The offsets to these two additional age-depth models were then combined with the uncertainty envelope originally derived for the first model to give a composite uncertainty reflective of the impacts of both random and correlated uncertainty.

The resulting age model for the entire lower part of CC8 is shown in Fig. 6 together with the 95% confidence interval. Although individual U–Pb 2σ age uncertainties ranged between values of 7.7–32.5 kyr (on average, about 1.5% of the determined age), the age-model uncertainties are in the range 3.9–12.2 kyr if the values before and after the two extreme age points are excluded (NB: lack of radiometric ages beyond the limits of the section results in an end-effect amplification of the age uncertainties). This equates to uncertainties between 0.4 and 1.3% of the modelled age. We now consider in detail the age uncertainties through each of the three glacial terminations represented in the lower section of CC8.

4.3.1. Age uncertainties through Termination X

Details of the age-depth model spanning Termination X, as well as the corresponding age uncertainty plot, are shown in Fig. 7a–b. According to the age-model results, this 88.5 mm long section grew continuously over a ~ 22 kyr period. Of the 15 U–Pb ages

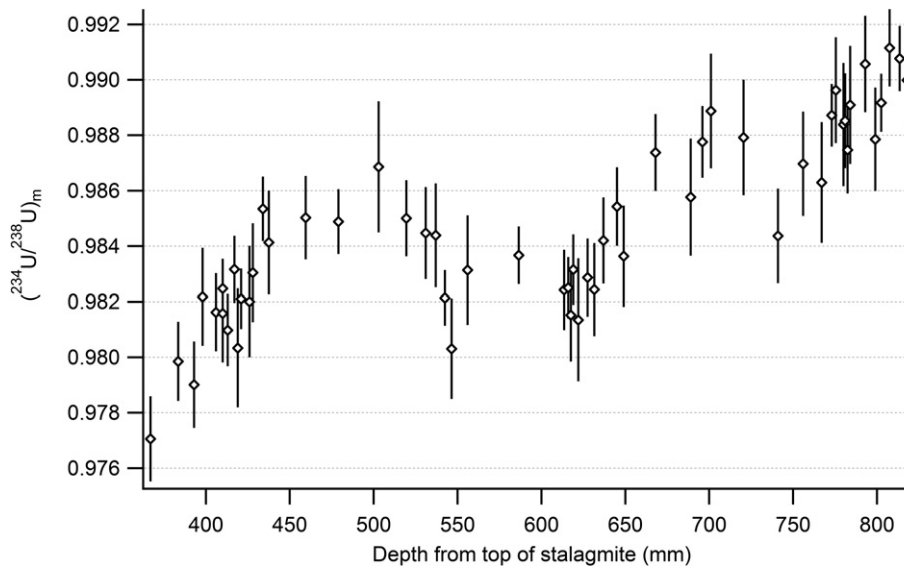


Fig. 5. $(^{234}\text{U}/^{238}\text{U})_m$ measurements were performed along the lower part of the CC8. $(^{234}\text{U}/^{238}\text{U})_m$ sample depth positions correspond to U–Pb sample positions. Although $(^{234}\text{U}/^{238}\text{U})_m$ is decreasing with time, the trend is not monotonic. This observed variability likely reflects changing hydrological conditions during different climate states, a subject of ongoing study at Corchia.

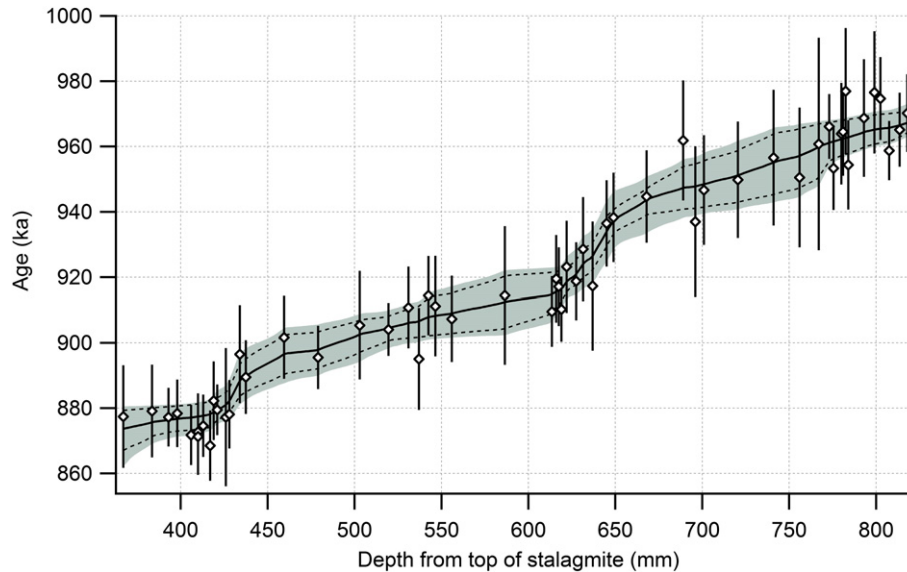


Fig. 6. Age-depth model for the older portion of CC8 based on 56 U–Pb dates and their associated uncertainties. The grey shaded area represents the 95% confidence age-model uncertainty envelope. Black dashed lines are age-depth models calculated using common Pb values of 0.8125 ± 0.0070 and 0.8265 ± 0.0070 and they are presented here to emphasize the effect of common Pb variability on final model ages. All U–Pb analyses returned ages in correct stratigraphic order when the age uncertainties of stratigraphically successive sample pairs are considered. The MSWD of 0.62 indicates that analytical uncertainties more than explain the observed scatter.

determined along this section, only one raw age deviates appreciably from the age model curve (CC8-59: 417 mm) but this still lies well within the overlapping 2σ age error bars of the neighbouring samples. The model age uncertainties range from 3.9 to 11.0 kyr, with highest values occurring at the youngest end of the section due to the end effect noted above: this is the youngest end of the age-depth model for the lower part of stalagmite CC8.

The section defining the start of Termination X is of greatest interest and is located around 877 ka. From the age uncertainty plot (Fig. 7b) it can be seen that model age uncertainties here are in the range 4.1–4.9 kyr, or 0.5–0.6% of modelled age.

4.3.2. Age uncertainties through Termination XI

The age model and age uncertainty plot for Termination XI is presented in Fig. 7c–d. With a length of 202.5 mm, this is the longest of all three sections and according to the mean modelled ages it spans ~ 45 kyr of time. Twenty samples were dated along this section. As with the T-X section, there is one clear outlying age-depth point but this overlaps with neighbouring samples within their respective uncertainties. Model age uncertainties along this section are in range from 4.9 to 9.7 kyr, or 0.5–1.1% of the corresponding model ages.

As can be seen in Fig. 7d, the model age uncertainties through the region where Termination XI commences are in the range of 7.3–7.5 kyr (i.e. 0.8% of the modelled age).

4.3.3. Age uncertainties through Termination XII

The lowest part of the stalagmite captures palaeoclimate information about Termination XII, the oldest termination preserved in CC8. Detail of the age-depth model for this 163.5 mm long section, as well as the age uncertainty plot, are shown in Fig. 7e–f. In Fig. 7e we can see that the U–Pb ages for this part of stalagmite are characterized by the highest U–Pb age uncertainties, particularly in the area from ~ 700 to 790 mm of depth. The age model is relatively poorly constrained in this part of the stalagmite, with uncertainties greater than 10 kyr. This reflects greater scatter in the ages determined at this depth.

According to our stable isotope data the onset of Termination XII occurred at ~ 963 ka, where the model age uncertainty is in the

range of 5.2–5.9 kyr (i.e. $\sim 0.6\%$ of the corresponding modelled ages).

5. Discussion

5.1. Factors influencing age-model precision and accuracy in CC8

Accurate, robust age models and minimised age uncertainties are crucial for the successful application of speleothem time-series to palaeoclimate problems. Total age uncertainties of 1% or less for speleothems in the range of the U–Th dating method are now commonly reported. However, our results show that accurate ages with a precision as low as 0.4% are possible for older speleothems dated by the U–Pb method. Achieving high precision and accuracy provides an opportunity to date some of the most prominent but as yet insufficiently explored palaeoclimate events of the Early Pleistocene, such as the shift from 40-kyr to 100-kyr glacial–interglacial cycles.

The low magnitude of the age uncertainties in CC8 can be attributed to a combination of the high U content, low common Pb, and readily quantifiable residual $^{234}\text{U}/^{238}\text{U}$ disequilibrium. Careful sample selection and thorough pre-screening procedures play a large role in satisfying the first two of these factors. Even in cases where U concentrations are lower than those at Corchia (see Woodhead et al., 2012, for a summary of typical U and Pb contents in speleothems), satisfactory ages and age models with reduced age uncertainties should be achievable provided common Pb concentrations are in the low ppb range.

Regardless of the raw uncertainties, densely dated records such as the one presented here (i.e. where the uncertainties of many age determinations overlap) can lead to final age-depth model uncertainties significantly smaller than those of their best individual uncertainties (e.g. Scholz et al., 2012). An important consideration in improving age-model precision by this means is to correctly identify and quantify all sources of random and correlated uncertainties. Here the biggest source of uncertainty is a common component of the assigned initial $^{207}\text{Pb}/^{206}\text{Pb}$ of the single-aliquot ages and so we have propagated this source of correlated uncertainty into the age model after completion of the age-depth

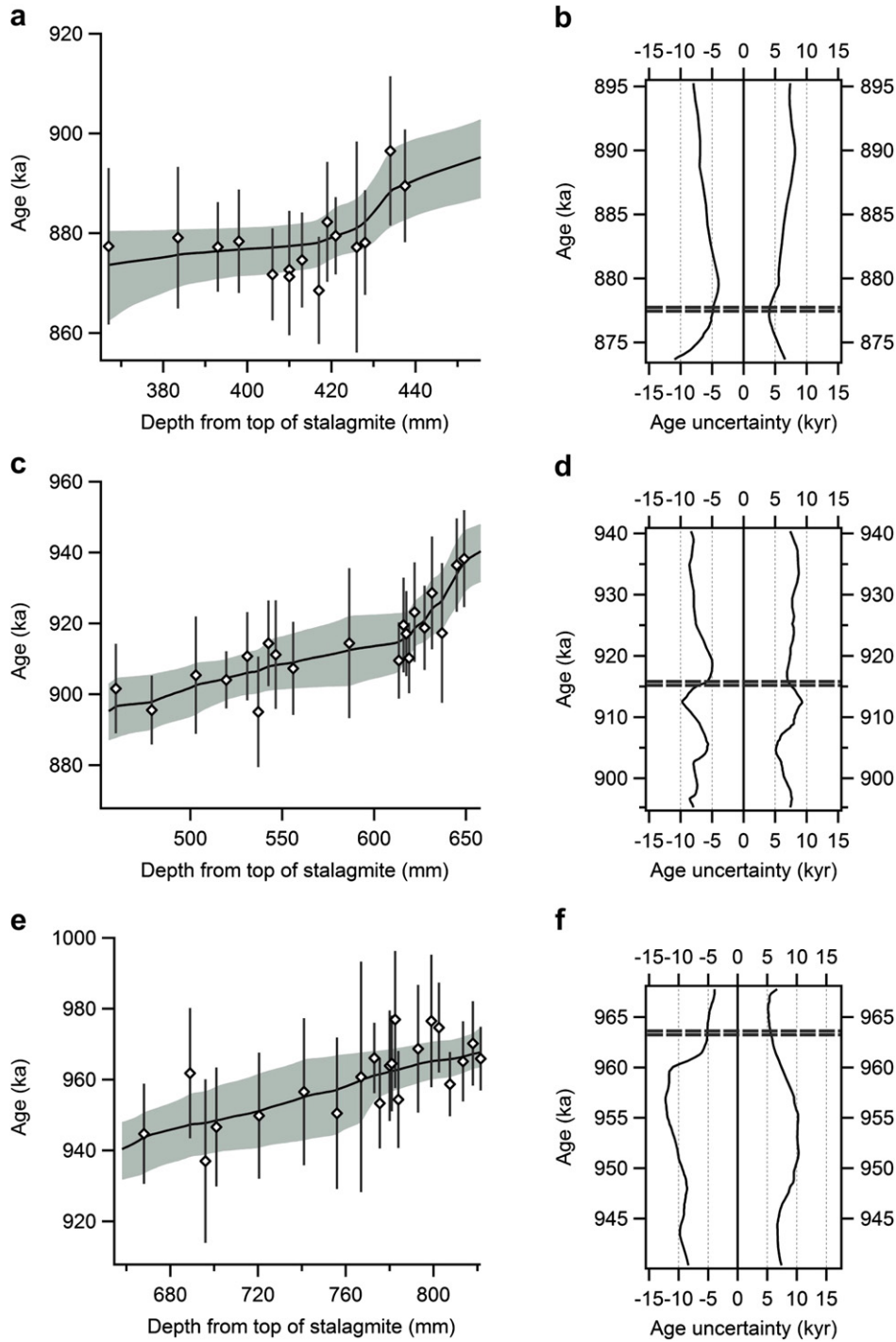


Fig. 7. (a, c, e) Details of the age–depth model through portions of CC8 where Terminations X, XI and XII are recorded, and the corresponding age–model uncertainty plots (b, d, f). Thick dashed lines on the uncertainty plots show the periods when terminations started according to our stable isotope data.

modelling process. An earlier version of the CC8 age–depth model depicted by Woodhead et al. (2012) did not consider the effect of correlated common uncertainty, which was exacerbated by the use of sparsely-constrained $^{234}\text{U}/^{238}\text{U}$ data rather than the per-sample measurement approach used here. This serves to illustrate the importance of per-sample measurement of $^{234}\text{U}/^{238}\text{U}$ where samples are sufficiently young that resolvable disequilibrium remains. Final sources of correlated age–model uncertainty to consider are spike calibration, decay constant and $\lambda^{238}\text{U}$ uncertainties. These are small compared to analytical and common Pb

uncertainties and do not significantly affect the age uncertainties reported here for CC8. They do, however, limit the age model uncertainties that could be theoretically achieved, to a little over 0.1%. Correlated uncertainties seem to be an important consideration in age–depth modelling in general and their impact is also likely to be of significance to U–Th chronologies in some cases, particularly where a non-trivial initial Th component is present.

Although U–Pb age uncertainties as low as 1–2% are readily achievable (Cliff et al., 2010; Meyer et al., 2009; Woodhead et al., 2006, 2010), another factor that controls the absolute magnitude

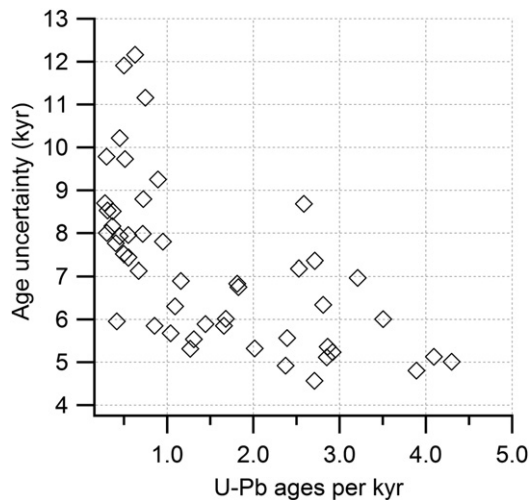


Fig. 8. Plot of age-model uncertainty versus age density. Here, density is expressed as the number of U–Pb modelled ages per kyr. Once a density of one age per kyr is achieved there is no significant improvement in age-model uncertainties.

of the age uncertainties is the time interval under consideration. Once age-model uncertainties move significantly beyond ~ 10 kyr (about half a precession cycle) the ability to make a first-order discrimination between the different orbital parameters disappears.

5.2. Age density versus age uncertainty

The final issue we discuss is the point at which the addition of further ages does not measurably improve the age model. On first viewing of the age-depth model (Fig. 6), it is obvious that the distribution of dated samples is unevenly spread throughout the section of the stalagmite. This was by design: our rationale here was to derive precise age-model solutions through specific palaeoclimate events. Hence, the sections of highest age density and thus in most cases lowest modelled age uncertainties correspond to these events. An important consideration in U–Pb dating of speleothems is estimating the density of ages that are required to achieve a certain level of age-model uncertainty. To address this, we derived a simple age-density function and compared this to age uncertainty. The model age and maximum model age uncertainty at the depth of each age determination were first derived by interpolation of the raw age-depth model; raw U–Pb ages were not used because of the scatter of mean ages along the depth profile. The age-density function was calculated as the inverse of the difference in kyr between each successive model-interpolated age, expressed as “dating samples per kyr”. When plotted against the maximum model age uncertainty achieved within each successive pair of age positions (Fig. 8), there is, overall, a negative correlation that is best described by a power function. From this plot, we can see that uncertainties of < 10 kyr can be achieved consistently once the sampling density reaches 0.8 (i.e. eight age determinations every 10 kyr), and that once a density of 2.0 is reached (i.e. two age determination per kyr) uncertainties of ~ 5 kyr are possible, although not consistently so. Thus, to establish the timing of a glacial termination during the late Early Pleistocene to a precision of 5–10 kyr, we suggest that a minimum of eight U–Pb determinations are necessary, assuming that a typical termination spans a 10-kyr interval and that the speleothem has similar characteristics to CC8, i.e. high U, low common Pb, and well-constrained $^{234}\text{U}/^{238}\text{U}$ and initial $^{207}\text{Pb}/^{206}\text{Pb}$. This represents considerable analytical effort, particularly if isochron ages are required.

Ultimately, this approach is limited by the impact of correlated uncertainty of the $^{207}\text{Pb}/^{206}\text{Pb}$ determination, and further progress can only be made by refinement of this parameter.

6. Conclusion

Although speleothems from the late Quaternary have been increasingly used in palaeoclimate research during the last few decades, exploration of the palaeoclimate potential of speleothems older than 500 ka has been hampered by an inability to produce accurate and precise ages. Further improvement of the U–Pb method and development of time series for older speleothems is recognized as one of the main scientific goals in speleothem palaeoclimate science (Fairchild and Baker, 2012). Our study on stalagmite CC8 from Corchia cave shows that this is well within the realms of possibility.

The palaeoclimate significance of stalagmite CC8 lies in the three Middle Pleistocene glacial terminations recognized from its stable isotope profile (not presented here). Our main goal in this study was to explore how precisely we can establish the timing of these events. To achieve this, 56 samples unevenly distributed along the lower portion of CC8 were dated by the U–Pb method (Woodhead et al., 2006). Five of these were isochron ages and the remaining 51 samples were single-aliquot ages determined using the common-Pb procedure of Woodhead et al. (2012) based on a common Pb composition calculated from the five isochrons plus a further two from the upper part of the stalagmite. For disequilibrium corrections we measured $^{234}\text{U}/^{238}\text{U}$ ratios for each age point.

With carefully selected samples from the key parts of the speleothem we developed an age-depth model that produced age uncertainties to just below 4 kyr (i.e. 0.4% of the accompanying modelled age, at a position through Termination XII). Although the dataset may still be refined, our analysis suggests age uncertainties of 4.1–4.9 kyr, 7.3–7.5 kyr and 5.2–5.9 kyr have been achieved for the onset of Terminations X to XII respectively. Coupled with ongoing refinements in the age model, this level of accuracy gives us a confidence that we can use CC8 to test orbital theories responsible for these terminations. Our results demonstrate the necessity for intensive U–Pb sampling to date late Early Pleistocene terminations. In spite of the large time and analytical effort involved in producing precise and accurate age models, a palette of significant palaeoclimate questions can now be addressed with this method.

Acknowledgements

We are most grateful for the support of the Gruppo Speleologica Toscana and the Gruppo Speleologico Lucchese during our field campaigns at Corchia Cave. This work was conducted under an Australian Research Council *Discovery Project* grant (2011–2013: #DP110102185). Dan Condon and an anonymous reviewer are thanked for their reviews, which greatly improved this manuscript, and QG editor David Richards for his editorial handling and further helpful suggestions. PB is the recipient of a PhD scholarship from the University of Melbourne.

Editorial handling by: D. Richards

References

- Baker, A., Genty, D., Dreybrodt, W., Barnes, W.L., Mockler, N.J., Grapes, J., 1998. Testing theoretically predicted stalagmite growth rate with recent annually laminated samples: implications for past stalagmite deposition. *Geochimica et Cosmochimica Acta* 62, 393–404.
- Baldini, J.U.L., 2010. Cave Atmosphere Controls on Stalagmite Growth Rate and Palaeoclimate Records, vol. 336. Geological Society, London. *Special Publications* 283–294.

- Baneschi, I., Piccini, L., Regattieri, E., Isola, I., Guidi, M., Lotti, L., Mantelli, F., Menichetti, M., Drysdale, R.N., Zanchetta, G., 2011. Mikroklima in hidrologija na nadmorski visini 800–900 m v jamskem sistemu monte Corchia: Prve ugotovitve in pomen za paleoklimatološke raziskave (Hypogean microclimatology and hydrology of the 800–900 m asl level in the Monte Corchia cave (Tuscany, Italy): preliminary considerations and implications for paleoclimatological studies). *Acta Carsologica* 40, 175–187.
- Borsato, A., Frisia, S., Fairchild, I.J., Somogyi, A., Susini, J., 2007. Trace element distribution in annual stalagmite laminae mapped by micrometer-resolution X-ray fluorescence: implications for incorporation of environmentally significant species. *Geochimica et Cosmochimica Acta* 71, 1494–1512.
- Cheng, H., Edwards, R.L., Broecker, W.S., Denton, G.H., Kong, X., Wang, Y., Zhang, R., Wang, X., 2009. Ice age terminations. *Science* 326, 248–252.
- Cliff, R.A., Spötl, C., Mangini, A., 2010. U–Pb dating of speleothems from Spannagel Cave, Austrian Alps: a high resolution comparison with U-series ages. *Quaternary Geochronology* 5, 452–458.
- de Ruiter, D.J., Pickering, R., Steininger, C.M., Kramers, J.D., Hancox, P.I., Churchill, S.E., Berger, L.R., Backwell, L., 2009. New *Australopithecus robustus* fossils and associated U–Pb dates from Cooper's cave (Gauteng, South Africa). *Journal of Human Evolution* 56, 497–513.
- Drysdale, R.N., Zanchetta, G., Hellstrom, J.C., Fallick, A.E., Zhao, J.X., Isola, I., Bruschi, G., 2004. Palaeoclimatic implications of the growth history and stable isotope ($\delta^{18}\text{O}$ and $\delta^{13}\text{C}$) geochemistry of a middle to late Pleistocene stalagmite from central-western Italy. *Earth and Planetary Science Letters* 227, 215–229.
- Drysdale, R.N., Zanchetta, G., Hellstrom, J.C., Fallick, A.E., Zhao, J.X., 2005. Stalagmite evidence for the onset of the last interglacial in southern Europe at 129 ± 1 ka. *Geophysical Research Letters* 32, 1–4.
- Drysdale, R.N., Zanchetta, G., Hellstrom, J.C., Fallick, A.E., McDonald, J., Cartwright, I., 2007. Stalagmite evidence for the precise timing of North Atlantic cold events during the early last glacial. *Geology* 35, 77–80.
- Drysdale, R.N., Hellstrom, J.C., Zanchetta, G., Fallick, A.E., Sánchez Goñi, M.F., Couchoud, L., McDonald, J., Maas, R., Lohmann, G., Isola, I., 2009. Evidence for obliquity forcing of glacial termination II. *Science* 325, 1527–1531.
- Drysdale, R.N., Paul, B., Hellstrom, J., Couchoud, L., Greig, A., Bajo, P., Zanchetta, G., Isola, I., Spötl, C., Baneschi, I., Regattieri, E., Woodhead, J., 2012. Precise micro-sampling of poorly laminated speleothems for U-series dating. *Quaternary Geochronology* 14, 38–47.
- Fairchild, I.J., Smith, C.L., Baker, A., Fuller, L., Spötl, C., Matvey, D., McDermott, F., 2006. Modification and preservation of environmental signals in speleothems. *Earth-science Reviews* 75, 105–153.
- Fairchild, I.J., Treble, P.C., 2009. Trace elements in speleothems as recorders of environmental change. *Quaternary Science Reviews* 28, 449–468.
- Fairchild, I.J., Baker, A., 2012. *Speleothem Science: From Process to Past Environments*. John Wiley & Sons, Chichester.
- Fleitmann, D., Cheng, H., Badertscher, S., Edwards, R.L., Mudelsee, M., Göktürk, O.M., Fankhauser, A., Pickering, R., Raible, C.C., Matter, A., Kramers, J., Tüysüz, O., 2009. Timing and climatic impact of Greenland interstadials recorded in stalagmites from northern Turkey. *Geophysical Research Letters* 36, L19707. <http://dx.doi.org/10.1029/2009GL040050>.
- Frumkin, A., Stein, M., 2004. The Sahara–East Mediterranean dust and climate connection revealed by strontium and uranium isotopes in a Jerusalem speleothem. *Earth and Planetary Science Letters* 217, 451–464.
- Goede, A., McCulloch, M., McDermott, F., Hawkesworth, C., 1998. Aeolian contribution to strontium and strontium isotope variations in a Tasmanian speleothem. *Chemical Geology* 149, 37–50.
- Griffiths, M.L., Drysdale, R.N., Gagan, M.K., Frisia, S., Zhao, J.X., Ayliffe, L.K., Hantoro, W.S., Hellstrom, J.C., Fischer, M.J., Feng, Y.X., Suwargadi, B.W., 2010a. Evidence for Holocene changes in Australian–Indonesian monsoon rainfall from stalagmite trace element and stable isotope ratios. *Earth and Planetary Science Letters* 292, 27–38.
- Griffiths, M.L., Drysdale, R.N., Vonhof, H.B., Gagan, M.K., Zhao, J.X., Ayliffe, L.K., Hellstrom, J.C., Hantoro, W.S., Cartwright, I., Frisia, S., Suwargadi, B.W., 2010b. Younger Dryas–Holocene temperature and rainfall history of southern Indonesia from $\delta^{18}\text{O}$ in speleothem calcite and fluid inclusions. *Earth and Planetary Science Letters* 295, 30–36.
- Hellstrom, J.C., McCulloch, M.T., 2000. Multi-proxy constraints on the climatic significance of trace element records from a New Zealand speleothem. *Earth and Planetary Science Letters* 179, 287–297.
- Hellstrom, J., 2003. Rapid and accurate U/Th dating using parallel ion-counting multi-collector ICP-MS. *Journal of Analytical Atomic Spectrometry* 18, 1346–1351.
- Hellstrom, J., 2006. U–Th dating of speleothems with high initial ^{230}Th using stratigraphical constraint. *Quaternary Geochronology* 1, 289–295.
- Hendy, E., Tomiak, P., Collins, M., Hellstrom, J., Tudhope, A., Lough, J., Penkman, K., 2012. Assessing amino acid racemization variability in coral intra-crystalline protein for geochronological applications. *Geochimica et Cosmochimica Acta* 86, 338–353.
- Lachniet, M.S., 2009. Climatic and environmental controls on speleothem oxygen-isotope values. *Quaternary Science Reviews* 28, 412–432.
- Ludwig, K.R., 1977. Effect on initial radioactive-daughter disequilibrium on U–Pb isotope apparent ages of young minerals. *Journal of Research of the U.S. Geological Survey* 5, 663–667.
- Ludwig, K.R., 2001. *A Geochronological Toolkit for Microsoft Excel. Isoplot/Ex, rev. 2.49*. Berkeley Geochronology Center, Berkeley, USA. Special Publication, 1a.
- McDermott, F., 2004. Palaeo-climate reconstruction from stable isotope variations in speleothems: a review. *Quaternary Science Reviews* 23, 901–918.
- Meyer, M.C., Cliff, R.A., Spötl, C., Knipping, M., Mangini, A., 2009. Speleothems from the earliest quaternary: snapshots of paleoclimate and landscape evolution at the northern rim of the Alps. *Quaternary Science Reviews* 28, 1374–1391.
- Meyer, M.C., Cliff, R.A., Spötl, C., 2011. Speleothems and mountain uplift. *Geology* 39, 447–450.
- Pickering, R., Kramers, J.D., 2010. Re-appraisal of the stratigraphy and determination of new U–Pb dates for the Sterkfontein hominin site, South Africa. *Journal of Human Evolution* 59, 70–86.
- Pickering, R., Kramers, J.D., Partridge, T., Kodolanyi, J., Pettke, T., 2010. U–Pb dating of calcite–aragonite layers in speleothems from hominin sites in South Africa by MC-ICP-MS. *Quaternary Geochronology* 5, 544–558.
- Pickering, R., Dirks, P.H.G.M., Jinnah, Z., de Ruiter, D.J., Churchill, S.E., Herries, A.I.R., Woodhead, J.D., Hellstrom, J.C., Berger, L.R., 2011. *Australopithecus sediba* at 1.977 Ma and implications for the origins of the Genus *Homo*. *Science* 333, 1421–1423.
- Polyak, V., Hill, C., Asmerom, Y., 2008. Age and evolution of the Grand Canyon revealed by U–Pb dating of water table-type speleothems. *Science* 319, 1377–1380.
- Raymo, M.E., Huybers, P., 2008. Unlocking the mysteries of the ice ages. *Nature* 451, 284–285.
- Richards, D.A., Bottrell, S.H., Cliff, R.A., Ströhle, K., Rowe, P.J., 1998. U–Pb dating of a speleothem of Quaternary age. *Geochimica et Cosmochimica Acta* 62, 3683–3688.
- Richards, D.A., Dorale, J.A., 2003. U-series chronology of speleothems and paleoclimate. Uranium-series geochemistry. *Reviews in Mineralogy and Geochemistry*, 407–460.
- Schmitz, M.D., Schoene, B., 2007. Derivation of isotope ratios, errors, and error correlations for U–Pb geochronology using ^{205}Pb – ^{235}U –(^{233}U)-spiked isotope dilution thermal ionization mass spectrometric data. *Geochemistry Geophysics Geosystems*. <http://dx.doi.org/10.1029/2006GC001492>.
- Scholz, D., Hoffmann, D., Hellstrom, J., Bronk Ramsay, C., 2012. A comparison of different methods for speleothem age modelling. *Quaternary Geochronology* 14, 94–104.
- Stirling, C.H., Esat, T.M., Lambeck, K., McCulloch, M.T., Blake, S.G., Lee, D.-C., Halliday, A.N., 2001. Orbital forcing of the marine isotope stage 9 interglacial. *Science* 291, 290–293.
- van Breukelen, M.R., Vonhof, H.B., Hellstrom, J.C., Wester, W.C.G., Kroon, D., 2008. Fossil dripwater in stalagmites reveals Holocene temperature and rainfall variation in Amazonia. *Earth and Planetary Science Letters* 275, 54–60.
- Walker, J., Cliff, R.A., Latham, A.G., 2006. U–Pb isotopic age of the StW 573 hominid from Sterkfontein, South Africa. *Science* 314, 1592–1594.
- Woodhead, J., Hellstrom, J., Maas, R., Drysdale, R., Zanchetta, G., Devine, P., Taylor, E., 2006. U–Pb geochronology of speleothems by MC-ICP-MS. *Quaternary Geochronology* 1, 208–221.
- Woodhead, J., Reisz, R., Fox, D., Drysdale, R., Hellstrom, J., Maas, R., Cheng, H., Edwards, R.L., 2010. Speleothem climate records from deep time? Exploring the potential with an example from the Permian. *Geology* 38, 455–458.
- Woodhead, J., Hellstrom, J., Pickering, R., Drysdale, R., Paul, B., Bajo, P., 2012. U and Pb variability in older speleothems and strategies for their chronology. *Quaternary Geochronology* 14, 105–113.
- Zanchetta, G., Drysdale, R.N., Hellstrom, J.C., Fallick, A.E., Isola, I., Gagan, M.K., Pareschi, M.T., 2007. Enhanced rainfall in the western Mediterranean during deposition of sapropel S1: stalagmite evidence from Corchia cave (central Italy). *Quaternary Science Reviews* 26, 279–286.
- Zhou, H., Feng, Y.X., Zhao, J.X., Shen, C.C., You, C.F., Lin, Y., 2009. Deglacial variations of Sr and $^{87}\text{Sr}/^{86}\text{Sr}$ ratio recorded by a stalagmite from central China and their association with past climate and environment. *Chemical Geology* 268, 233–247.